

PACS numbers: 42.62.Be; 42.30.Wb
DOI: 10.1070/QE2004v034n12ABEH002800

Visualisation of human subcutaneous blood vessels by increasing coherence probing depth

S.G. Proskurin, R.K. Wang

***Abstract*. An improved Fourier-domain rapid-scanning optical delay line in the reference arm of a Michelson interferometer is described which allows the use of a low-power superluminescent diode (down to 0.2 mW) and of a few wavelengths simultaneously. The method of raster scanning and averaging in the sample arm of the interferometer within a pixel provides an additional increase in the signal-to-noise ratio by 4 – 10 dB and, in combination with optical clearing, an increase in the coherence probing depth for the human skin *in vivo* up to 1.5 – 1.6 mm. As a result, subcutaneous blood vessels are visualised for the first time and a signal from the bloodstream is detected in the transitional regime between reflected and diffusively scattered photons. The images of subcutaneous blood vessels of the human palm and finger *in vivo* are presented. The possibility of construction of a low-coherence Doppler spectrograph with a variable coherence length is discussed.**

Keywords: *coherence probing depth, optical low-coherence tomography, Doppler spectroscopy and anemometry, optical properties of skin, optical clearing of tissues, blood vessels.*

1. Introduction

It is known that optical low-coherence reflectometry [1, 2] uses the principles of scanning low-coherence interferometry [3]. The low coherence ($\lambda^2/\Delta\lambda$) of a pulsed or continuous wave (cw) radiation source is caused by its broad spectral band, which gives a high spatial resolution

$$\Delta z = \frac{2\ln 2}{\pi}\frac{\lambda^2}{\Delta\lambda} \approx 0.44\frac{\lambda^2}{\Delta\lambda}$$

in the sample arm in scanning interferometers. The longitudinal component Δz of the measurement volume (spatial resolution over the probing depth) achieves 5 – 15 μm when cw superluminescent diodes (SLDs) are used ($\lambda = 800 - 1700$ nm, $\Delta\lambda = 20 - 100$ nm). Such a short coherence envelope from a cw source corresponds to a laser pulse of duration 15 – 50 fs. By considering the propagation of radiation in biological tissues, it is necessary to take into account their refractive index $n \approx 1.4$ [4], which gives the axial spatial resolution in the tissue [by probing over the depth (A-scan)] $L_{ax} = \Delta z/n \approx 4{-}11$ μm. Low-coherence reflectometry allows the visualisation of strongly scattering tissues over a depth of 0.5 – 1.0 mm with this resolution. The method called optical low-coherence tomography (OCT) has received wide applications in biomedicine for the last fifteen years [5]. As a rule, OCT techniques use a scanning Michelson interferometer based on single-mode fibres (Fig. 1) or a Linnik microscope [3, 6].

Compared to quasi-elastic scattering, when a narrow-band radiation source (laser) with $\Delta\lambda = 0.1 - 1.0$ nm is used, a detector in the low-coherence scheme detects, apart from the interference signal, also an incoherent spurious signal, which is manifested as a phase noise [1, 2].

The detection of light from the reference and signal arms of the interferometer

$$E_r = E_r\cos(kz_r + \varphi_1) \text{ and } E_s = E_s\cos(kz_s + \varphi_2)$$

with a quadratic receiver gives

$$I = \langle E_r E_s\rangle = I_{in} + E_r^2 + E_s^2 + 2E_rE_s \times \cos[2\pi f_0 t + (\varphi_1 - \varphi_2)] = I_{in} + I_rI_s + 2(I_rI_s)^{1/2}\cos(2\pi f_0 t + \Delta\varphi(t)),$$

where I_{in} is a new incoherent component. The maximum contrast of the interference pattern, when a coherent source is used, which is commonly employed for studying quasi-elastic scattering, is achieved for $I_r = I_s$. In the regime of optical heterodyning, it is necessary to increase the intensity I_r of the reference wave. An increase in the intensity and efficient filtering of the low-frequency component $I_r + I_s$ leads to the rise in the intensity of the component at the carrier frequency of the interferometer corresponding to the Doppler frequency

$$f_0 = \frac{2V}{\lambda}$$

of the mirror of the reference arm linearly scanning at the velocity V. When such a linearly scanning optical delay line (ODL) is used, the pass band Δf of the filter of a signal amplifier should be chosen in accordance with the linewidth of a broadband radiation source ($\Delta\lambda \approx 20 - 300$ nm):

S.G. Proskurin, R.K. Wang Cranfield University, Silsoe, Bedfordshire, MK45 4DT, United Kingdom; e-mail: s.g.proskurin@cranfield.ac.uk

Received 13 May 2004
Kvantovaya Elektronika **34** (12) 1157 – 1162 (2004)
Translated by M.N. Sapozhnikov

$$\Delta f = f_0(\Delta\lambda/\lambda_0).$$

When a rapid-scanning ODL based on a diffraction grating and an angle-scanning mirror is used [7, 8], the pass band Δf additionally broadens approximately by a factor of four [7, 9]:

$$\Delta f = 4\frac{\Delta\lambda}{\lambda^2}\left(\Delta x - \frac{L_f\lambda}{d}\right)\frac{\partial\alpha}{\partial t},$$

where L_f is the focal distance of a lens; α is the scan angle of the mirror; and d is the grating pitch. The carrier frequency takes the form

$$f_0 = \frac{4\Delta x}{\lambda}\frac{\partial\alpha}{\partial t}.$$

The frequency of a rapid-scanning ODL achieves several kilohertz, which allows one to obtain a few tens of OCT images per second. In this case, the carrier frequency and its broadening become very large, and therefore the resolution and coherent probing depth decrease. The image contrast cannot be increased with the help of usual filtration at high scan rates. We managed to reduce the focal distance L_f and modify the rapid-scanning ODL, which allowed us to reduce substantially the intensity of the radiation source (SLD) [10]. The decrease in L_f also gave the possibility to control the varying intensity in the reference arm.

2. Doppler methods

Doppler optical low-coherence tomography (DOCT) [11–14] expands the functional possibilities of OCT and allows one to obtain not only the structural image of an object but also two-dimensional velocity distributions in flows in cylindrical capillaries [11, 12] and in flows with a complex geometry [15–17]. At present DOCT is more widely used than laser Doppler anemometry (LDA) and microscopy (LDM) [18, 19].

DOCT offers a number of substantial advantages over LDA, however, the Doppler shift detected by this method (a few kilohertz) corresponds to the velocity of particles equal to a few millimetres per second. Such frequencies and velocities are two-three order of magnitude greater than those detected with a sign-sensitive laser Doppler microscope, which can detect frequency changes at the level of several hertz, which corresponds to velocities of the order of a few micrometres per second. A velocity sign-sensitive microscope with such a resolution is in fact a laser Doppler spectrometer (LDS) [20]; however, the measurement volume is localised in the microscope by mean of a focusing optics and an aperture.

To eliminate the relation

$$\Delta f_D = 2\Delta V/\lambda$$

between the spatial and velocity distribution in DOCT, it was proposed, similarly to ultrasound colour Doppler velocimetry, to find the phase shift in consecutive A-scans, when flow velocities are rather small ($0.01-1$ mm s^{-1}). In this method, the ratio of the phase shift to the time Δt between the consecutive A-scans is determined:

$$\Delta f_D = 2\Delta\varphi/(2\pi\Delta t).$$

As the scan rate is increased, the values of f_0 and Δf increase, however, Δt decreases, which should improve the velocity measurement accuracy approximately to 10 μm s^{-1} [13, 14]. However, the spatial resolution $L_{ax} = 10$ μm corresponds, by definition, to the phase interruption after approximately each 30 fs, and the adjacent A-scans can be detected only after $10^{-2}-10^{-7}$ s. To overcome this problem, the coherent modulation of the radiation phase by means of an electro-optical modulator is used [14]. Such an approach, called colour Doppler tomography, is mainly used to visualise the bloodstream velocity in a human eye retina [21].

Doppler spectra obtained in DOCT are usually rather broad and irregular; however, the average velocity of particles in the measurement volume can be determined with a comparatively small error (2 %–5 %), which became an important experimental achievement [13]. We proved experimentally that, despite a rather large broadening (up to several kilohertz), DOCT spectra are symmetric and their shape is well described by a Gaussian with an accuracy of 1 %–2 % [17]. This is explained by the fact that the OCT method detects mainly a signal reflected back from particles whose velocity distribution in the measurement volume is Gaussian. The LDS detects spectra of quasi-elastic scattering from the entire volume of particles, which are rather complicated, especially in the case of biological liquids, for example, blood and protoplasm [18, 19].

3. Ultimate resolution of coherent probing

When femtosecond lasers ($\lambda = 800-1000$ nm, $\Delta\lambda = 100-350$ nm) and thermal radiation sources are used, the spatial resolution achieves 1 μm [3, 6, 21, 22]. Such systems allow the visualisation of even individual regions of a cell, but only in the case of translucent, weakly scattering objects. The probing depth is 0.3–0.6 μm, which is twice as large as that for a confocal microscope [23, 24]. Note that femtosecond lasers emitting at a wavelength of above 1000 nm are not available so far, while the maximum penetration depth of radiation in biological tissues can be achieved at a wavelength of ~ 1300 nm [4]. In addition, the dispersion of the coherence envelope of length less than 3 μm in a biological tissue only reduces the probing depth.

4. Experimental setup

We used a standard scanning Michelson interferometer based on single-mode IR fibres (Fig. 1). Radiation from SLD (*1*) ($\lambda = 1298$ nm, $\Delta\lambda = 52$ nm) was coupled to 50 : 50 fibre beamsplitter (*2*) and then to 50 : 50 fibre beamsplitter (*3*). One-half radiation from the latter is coupled to the reference arm of the interferometer and another half to its sample arm and is focused on an object with a system of lenses. Radiation reflected from the interferometer arms is mixed in quadratic photodetectors PD1 and PD2 in the balance circuit. In this circuit, the interference signal is detected in phase (summed), whereas the excess photon noise and vibrations of the system are detected out-of-phase (subtracted). The electric signal from the balance circuit is fed to a band-pass filter and then to a spectrum analyser and a 12-bit analog-to-digital converter (ADC). The ADC output digital signal is recorded and computer-processed.

Rapid-scanning optical delay (RSOD) (Fig. 2) was

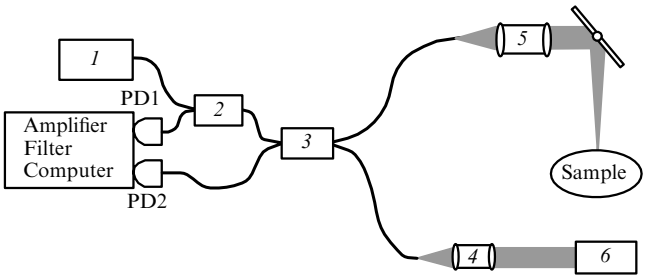

Figure 1. Scheme of a scanning Michelson interferometer based on single-mode fibres: (*1*) SLD; (*2*, *3*) fibre beamsplitters (1×2 and 2×2, respectively); (*4*) collimator; (*5*) focusing lens system; (6) rapid-scanning ODL; (PD1 and PD2) IR photodetectors in a balance scheme.

developed for studying the shape and duration of ultrashort laser pulses [7], which assumes the use of high-power radiation sources. We have made for the first time [10, 17] the RSOD operating at radiation powers in each of the arms of the interferometer reduced to ~ 0.1 mW. As the SLD power is further decreased, the SLD noise becomes comparable with the electric noise of the amplifier and the signal-to-noise ratio is not improved.

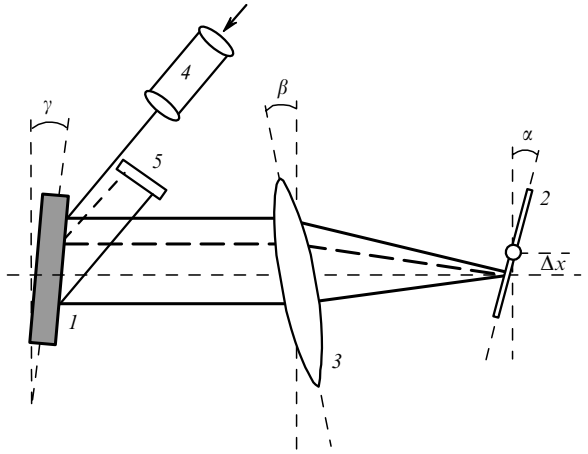

Figure 2. Modified rapid-scanning optical delay line based on diffraction grating (*1*) and scanning mirror (*2*) located in the focal plane of lens (*3*) with a small displacement Δx from the optical axis; (*4*) collimator; (*5*) double-pass mirror; α, β, γ are the tilt angles of the mirror, lens, and grating, respectively, which are varied during adjustment.

Radiation from a collimator is incident on a diffraction grating, then on the edge of a focusing lens and on a scanning mirror. Backward radiation is scanned through the lens centre, is diffracted from the diffraction grating, is incident on a double-pass mirror, and reflecting from it, returns along the same path. By varying the angles of the scanner, lens, and grating (α, β, and γ respectively), we can reliably adjust the RSOD. The improved RSOD allows us to use simultaneously both wavelengths (1.3 and 1.5 μm), only with a small deterioration of the image contrast (10 % – 15 %). The successive use of both wavelengths requires a slight control of the tilt angle γ of the grating, the image contrast increasing in this case by the same 10 % – 15 %. It is obvious that any other wavelengths can be used in this spectral range.

To obtain differential images, two wavelengths are required. This approach was realised in the study of an eye cornea with the help of a linearly scanning mirror [25].

Scanning in the sample arm. To obtain a two-dimensional image (B-scan), scanning in the second arm (Fig. 1) is also performed by means of a scanning mirror. The use of such a raster scanning, unlike one-dimensional scanning to the left and right with the help of an object table, allows one to perform raster averaging within one pixel, thereby reducing the above-mentioned noise and the speckle noise appearing due to the spatial coherence of the SLD during multiple scattering of radiation in a sample [26, 27]. Such a raster averaging additionally improves the signal-to-noise ratio by 4 – 10 dB.

By using the focusing optics with a smaller numerical aperture NA, we increased the confocal parameter to the size corresponding to the signal penetration depth 2 – 3 mm. In this case, the beam waist diameter

$$\Delta w = \frac{0.61\lambda}{\mathrm{NA}}$$

increased up to 30 – 80 μm. This reduces the transverse resolution, but such a resolution is quite sufficient for the visualisation of a layered structure like a skin. In addition, a smaller numerical aperture of the focusing optics eliminates the entry of photons multiply scattered at large angles on the detector and allows the separation of only reflected and backscattered component, which contains information on the object structure. In this case, the axial resolution L_{ax} is still determined by the source coherence and remains equal to approximately 10 μm.

Signal processing. The recorded interference signal consists of 100 – 200 A-scans. Each of the lines is processed using the fast Fourier transform, the moving window of the Fourier transform selecting from the interferogram N points with the displacement $\sim 20\,\% - 80\,\%$ of the window length. The window equal to $2^n = N$ points should best correspond to the coherence envelope length (Fig. 3) determining the resolution L_{ax} of the interferometer. Because the path difference between the interferometer arms changes continuously during the ODL scan, the window of the Fourier transform also should theoretically shift continuously, i.e., by one point, which makes signal processing quite long (of

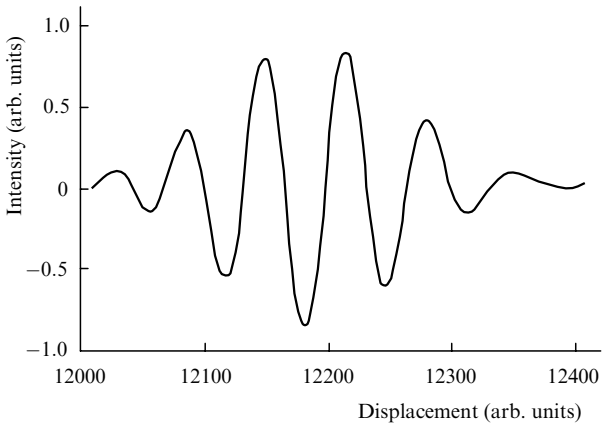

Figure 3. Coherent envelope of low-coherence continuous radiation obtained by placing a reflecting plate to the sample arm. The envelope length corresponds to the resolution ~ 15 μm in free space.

the order of several minutes). It was found empirically that signal processing with the window displacement by 20 % – 30 % gives the same image contrast as in the case of a continuous displacement by one point, but takes only 1 – 2 s (when a 2.4-GHz Pentium 4 processor is used). By using special software written in the C++ language, this time can be reduced to 1 s and less. In this case, digital processing can be performed parallel with the signal reading [28]. Such an approach provides real-time imaging and visual feedback in the studies of living objects.

5. Results

We have built and introduced to clinics three OCT setups using SLDs emitting in the range from 0.8 to 1.5 μm (Fig. 4). Subcutaneous blood vessels were visualised using reasonably a 1.3-μm SLD. Note that OCT with a rapid-scanning ODL and $\lambda \approx 1.5$ μm (Fig. 4c) was realised for the first time.

By using the above-described method and optical clearing, we managed for the first time to obtain the image of a subcutaneous blood vessel of diameter 0.2 – 0.5 mm at a depth of 1 – 1.6 mm for 1 – 5 s [17]. After several carpal movements of a hand, we observed for the first time the signal from the bloodstream [10]. Figure 5 shows the blood vessels of a finger located at a depth of 1 – 1.6 mm, which were imaged before and after optical clearing produced by a fourfold application of a biologically neutral solution of glycerol with water on the skin surface for 15 min [29, 30]. The blood vessel was imaged (Fig. 5a) at the 80-Hz scan rate, corresponding to the detection time ~ 2.2 s upon reading each next (even or odd) A-scan and to ~ 1.1 s upon reading both lines (even and odd). By increasing the scan rate up to a few kilohertz, one can obtained the video regime with a frame rate of 10 – 30 frames per second; however, in this case the coherence probing depth was insufficient for visualisation of subcutaneous blood vessels [9, 28]. Figures 5b, c show the images of the same blood vessel obtained after optical clarification. The image in Fig. 5b was obtained after raster averaging over four lines within one pixel. The scan rate in the object arm is reduced by a factor of four, which increases proportionally the signal detection time but substantially reduces the speckle noise [26, 27] and enhances the image contrast due to the increase in the signal-to-noise ratio by 4 – 10 dB because of the raster averaging of individual A-scans.

The processing of individual A lines showed also that the axial resolution gradually deteriorated from the theoretical value 10 μm to 30 – 50 μm. This means that weakly back-scattered radiation, which remains coherent to radiation of the reference arm of the interferometer, is detected. This transitional OCT mode allows the coherence probing depth to be increased up to 1 – 1.6 μm, where the conventional detection of reflected photons cannot be realised.

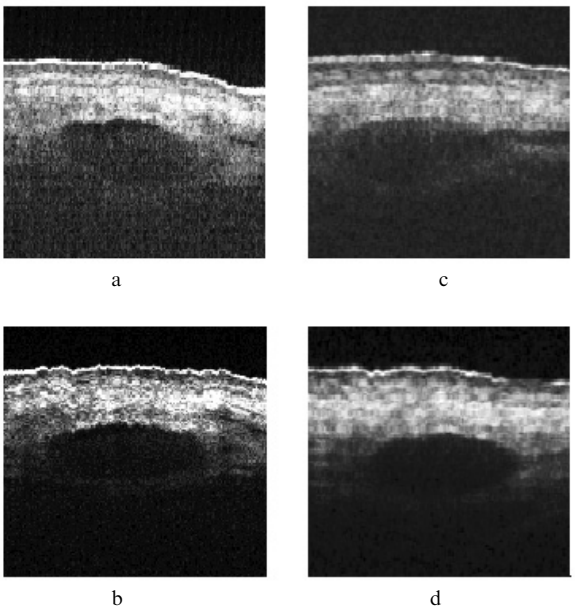

Figure 5. OCT images of the cross section of two blood vessels of a Y-junction in a finger of an adult obtained before (a, c) and after (b, d) optical clearing. The size of images is 2 × 2 mm.

Figure 6a shows the optical image of a section of the palm skin of an adult. The upper skin layers (stratum cornea, epidermis, derma), which have been observed many times, are well discernible. At a depth of ~ 0.6 mm and deeper, other subcutaneous structures become discernible, but the image is strongly blurred. To enhance the image contrast and increase the probing depth, we used, as in the previous case, the method of optical clearing. Figure 6b shows the image of the same region of the skin, but obtained with a much better contrast. At a depth of $\sim 1.1 - 1.4$ mm, structures in the form of circles are discernible (shown by the arrow), which are blood vessels. Figure 6c shows the same region imaged within 30 min after the beginning of clearing. The image contrast decreased and the bloods were no longer observed; however, the coherence probing depth increased: the signal was detected from a depth of $1.5 - 1.6$ mm, but with the spatial resolution that was worse by a factor of $4 - 6$.

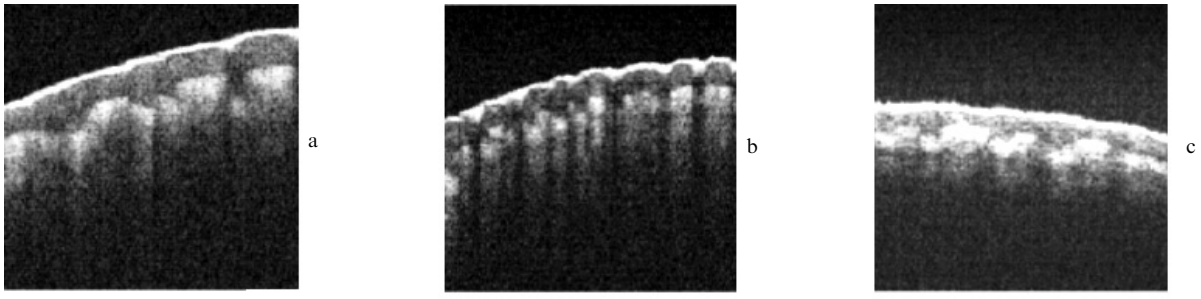

Figure 4. OCT image of a finger *in vivo* obtained by using SLDs emitting at ~ 0.8 μm ($\lambda = 840$ nm, $\Delta\lambda = 50$ nm) (a), ~ 1.3 μm ($\lambda = 1298$ nm, $\Delta\lambda = 52$ nm) (b), and ~ 1.5 μm ($\lambda = 1482$ nm, $\Delta\lambda = 61$ nm) (c). The image size is 2 × 2 mm.

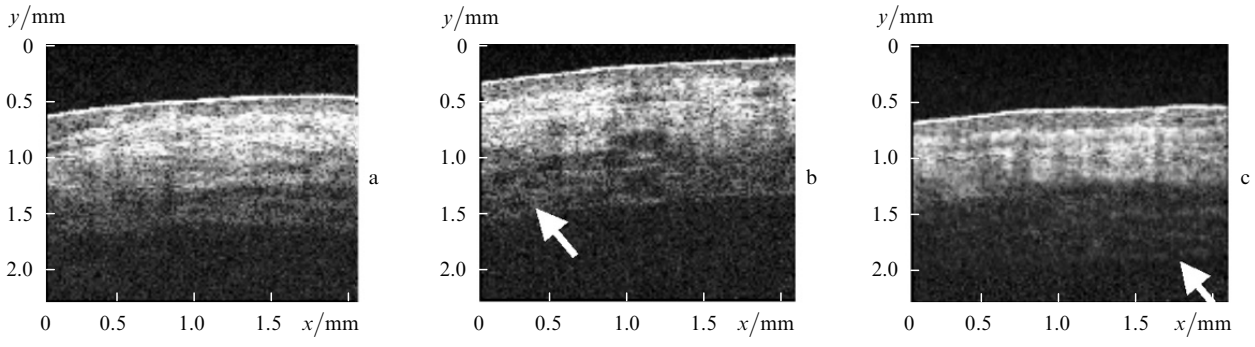

Figure 6. OCT images of a skin region on a palm of an adult obtained before optical clearing (a) and within 15 min (b, blood vessels are indicated by the arrow) and 30 min after clearing (c, blood vessels are not observed, the resolution is reduced to 50 μm, while the coherence probing depth increased to 1.5–1.6 mm).

6. Discussion of results

An increase in the numerical aperture of a lens in the sample arm of the interferometer, which is commonly used in traditional OCT, provides the resolution $L_{ax} \approx 3 - 10$ μm at a depth of 0.6–0.9 mm, which exceeds approximately by two-three times the possibilities of confocal microscopy [9, 14, 28]. When the imaging time is rather long (~ 4 s) (Fig. 5b), even microscopic tremor of the hand of a patient deteriorates the quality of the image of upper layers, which become blurred. The tremor does not affect the quality of images of the layers lying deeper than 0.5–0.6 mm. The resolution in the tissue at the depth more than 0.5–0.6 mm is the same for all the cases presented, although vibrations with the amplitude 10–20 μm are superimposed on the images of the upper layers. This is caused by a substantially lower spatial resolution of the visualisation of deep layers, so that the latter can be visualised only by using the transitional quasi-diffusion coherence mode of photon detection. The decrease in the resolution upon imaging lower layers by a factor of 3–5 compared to imaging upper layers is caused by radiation scattering and by a passage to the transitional mode between coherence and diffusion tomography. This is the regime of weakly scattered photons, which preserve coherence with the signal from the reference arm of the interferometer [10].

By changing the coherence of the source, we can obtain the correspondence between the length of the coherence envelope and the spatial resolution in deep layers of the object. In addition, this can be achieved by placing a dynamically changing aperture to the focal plane of the lens (Fig. 2), which is the Fourier plane of the scanning delay line. By increasing the source power and narrowing down a slit aperture, one can also use this OCT scheme in the regime of a Doppler spectrograph. This would give the possibility to compare quantitatively the operation of a Doppler spectrograph with that of a conventional Doppler microscope [18, 19] and to realise coherent Doppler spectrometry with a tunable coherence length.

7. Conclusions

We have used in our study an improved Fourier-domain rapid-scanning optical delay based on the use of a diffraction grating. The improvements described in the paper are important from the practical point of view because they allow one to reduce the RSOD dimensions to $10 \times 3 \times 5$ cm and to use a low-coherence radiation source such as an SLD of power down to 0.4 mW. The use of an optical isolator provides almost complete elimination of the reverse effect of radiation on the SLD and permits the decrease of the radiation source power by half. Raster averaging within one pixel enhances the signal-to-noise ratio by 4–10 dB. This allowed us to detect photons in the transitional mode from reflection and backscattering to the diffusion multiple scattering. Taking into account the optical properties of tissues *in vivo* [4], it is reasonable to assume that the coherence probing depth for weakly scattered photons can be further increased up to 2–3 mm. This is related to the fact that after a photon propagated 20–30 mean free paths [31], the ballistic component of the signal becomes comparable with the diffusion component, which means a passage to the regime of diffusion optical tomography.

Acknowledgements. The authors thank the Government of Her Royal Highness the Queen of England for the support of this study (Grant GR/R06816/02 of The Engineering and Physical Sciences Research Council (EPSRC)).

References

1. Youngquist R.C., Carr S., Davies D.E.N. *Opt. Lett.*, **12**, 158 (1987).
2. Takada K., Yokohama I., Chida K., Noda J. *Appl. Opt.*, **26**, 1603 (1987).
3. Linnik V.P. *Proc. Acad. Sci. USSR*, **1**, 208 (1933).
4. Tuchin V., in *Tissue Optics: Light Scattering Methods and Instruments for Medical Diagnostics*. Ed. by D.C.O'Shea (Bellingham, USA: SPIE Press, 2000) Vol. TT38, pp 42–44.
5. Huang D., Swanson E.A., Lin C.P., Schuman J.S., Stinson W.G., Chang W., Hee M.R., Flotte T., Gregory K., Puliafito C.A., Fujimoto J.G. *Science*, **254**, 1178 (1991).
6. Dubois A., Moneron G., Grieve K., Boccara A.C. *Phys. Med. Biol.*, **49**, 1227 (2004).
7. Kwong K.F., Yankelevich D., Chu K.C., Heritage J.P., Dienes A. *Opt. Lett.*, **18**, 558 (1993).
8. Tearney G.J., Bouma B.E., Fujimoto J.G. *Opt. Lett.*, **22**, 1811 (1997).
9. Rollins A., Izatt J., Kulkarni M., Yazdanfar S., Ung-arunyawee R. *Opt. Expr.*, **3**, 219 (1998).
10. Proskurin S.G., He Y., Wang R.K. *Opt. Lett.*, submitted.
11. Wang X., Milner T.E., Chen Z., Nelson S. *Appl. Opt.*, **36**, 144 (1997).
12. Izatt J.A., Kulkarni M.D., Yazdanfar S., Barton J.K., Welch J. *Opt. Lett.*, **22**, 1439 (1997).

13. Chen Z., Zhao Y., Srinivas S.M., Nelson J.S., Prakash N., Frostig R.D. *IEEE J. Sel. Top. Quantum Electron.*, **5**, 1134 (1999).
14. Zhao Y., Chen Z., Saxer C., Xiang S., de Boer J.F., Nelson J.S. *Opt. Lett.*, **25**, 114 (2000).
15. Proskurin S.G., Sokolova I.A., Wang R.K. *Phys. Med. Biol.*, **48**, 2907 (2003).
16. Proskurin S.G., He Y., Wang R.K. *Phys. Med. Biol.*, **49**, 1265 (2004).
17. Proskurin S.G., He Y., Wang R.K. *Proc. SPIE Int. Soc. Opt. Eng.*, **5330**, 38 (2004).
18. Proskurin S.G., Priezzhev A.V., Lapteva N.B. *Proc. SPIE Int. Soc. Opt. Eng.*, **2082**, 78 (1993).
19. Proskurin S.G. *Cand. Diss.* (Moscow: Moscow State University, 1993).
20. Akhmanov S.A., Nikitin S.Yu. *Physical Optics* (Oxford University Press, 1997) p. 345.
21. Drexler W. *J. Biomed. Opt.*, **9**, 47 (2004).
22. Drexler W., Morgner U., Kartner F.X., Pitris C., Boppart S.A., Li X.D., Ippen E.P., Fujimoto J.G. *Opt. Lett.*, **24**, 1221 (1999).
23. Izatt J.A., Hee M.R., Owen G.M., Swanson E.A., Fujimoto J.G. *Opt. Lett.*, **19**, 590 (1994).
24. Fujimoto J.G. *Private communication* (Cranfield University, Silsoe, UK, 2003).
25. Pircher M., Gotzinger E., Leitgeb R., Fercher A.F., Hitzenberger C.K. *Opt. Exp.*, **11**, 2190 (2003).
26. Schmitt J.M. *Phys. Med. Biol.*, **42**, 1427 (1997).
27. Schmitt J.M., Xiang S.H., Yung K.M. *J. Biom. Opt.*, **4**, 95 (1999).
28. Park B.H., Pierce M.D., Cense B., de Boer J.F. *Opt. Exp.*, **11**, 782 (2003).
29. Bashkatov A.N., Genina E.A., Korovina I.V., Kochubey V.I., Sinichkin Yu.P., Tuchin V.V. *Proc. SPIE Int. Soc. Opt. Eng.*, **4224**, 300 (2000).
30. Meglinskii I.V., Bashkatov A.N., Genina E.A., Churmakov D.Yu., Tuchin V.V. *Kvantovaya Elektron.*, **32**, 875 (2002) [*Quantum Electron.*, **32**, 875 (2002)].
31. Hee M.R., Izatt J.A., Jacobson J.M., Fujimoto J.G., Swanson E.A. *Opt. Lett.*, **18**, 950 (1993).